Proceedings of the 9th International Conference on Neural Information Processing (ICONIP'02), Vol. 5
Lipo Wang, Jagath C. Rajapakse, Kunihiko Fukushima, Soo-Young Lee, and Xin Yao (Editors)

SEGMENTATION OF PATHOLOGICAL FEATURES IN MRI BRAIN DATASETS

F. Kruggel, C. Chalopin, X. Descombes, V. Kovalev

Max-Planck-Institute of Cognitive Neuroscience
Stephanstraße 1, D-04103 Leipzig, Germany
email: kruggel@cns.mpg.de

Jagath C. Rajapakse

School of Computer Engineering
Nanyang Technological University
Singapore 639798 email: asjagath@ntu.edu.sg

ABSTRACT

One of the major clinical applications of magnetic resonance imaging (MRI) is to detect pathological features in human body parts. While results are available in a digital format, their evaluation is performed by a trained human observer, which is still considered as the "gold standard". However, providing additional quantitative figures (e.g., lesion size or count) is tedious for a human and may better be obtained from automatical image processing methods. Three example brain lesion types (as revealed by MRI) and methods for their detection are described. Special emphasis is led on the way prior knowledge about the specific lesion type is incorporated in the algorithm.

1. INTRODUCTION

Detecting pathological features in magnetic resonance imaging (MRI) data sets of the human head is considered a non-trivial segmentation task. Segmentation approaches require prior knowledge about the lesion charactistics (e.g., their expected compartment, size and shape, their signal statistics in relation to the embedding tissue), and thus, are generally targeted for detection of a specific lesion type (e.g., [9, 13]). For historical reasons and their medical significance, most approaches focused on white matter lesions due to Multiple Sclerosis (e.g., [7]), while methods for segmenting large focal lesions appeared only recently (e.g., [6]).

Herein, we focus on approaches that are targeted to automatically detect (a) large unilateral lesions, (b) small multifocal lesions, and (c) diffuse white matter lesions. While a trained human observer is still outperforming automatic approaches for lesion detection and discrimination, estimating the lesion size (in the case of large unilateral or diffuse lesions), count and position (in the case of multifocal lesions) is tedious or even impossible.

The aim of this work is to provide quantitative descriptors for different lesion types. According to their properties, different approaches were found useful. Especially, these three example algorithms incorporate prior knowledge in fundamentally different ways, as explained in more detail below. The quantitative descriptors may be considered as useful measures in statistical evaluations of a patient's clinical status.

2. SEGMENTATION OF FOCAL BRAIN LESIONS

Focal brain lesions are a consequence of head trauma, cerebral infarcts or intracerebral hemorrhages. Properties of the lesion (i.e. position, extent, density) are known to be related to cognitive handicaps of a patient. Visual examination of the lesions suffers from inter- and intra-observer variability [13]. Semi-automatic or automatic methods for analyzing lesions in MR data sets are advantageous because consistent and reproductible criteria are employed to yield quantitative lesion descriptions.

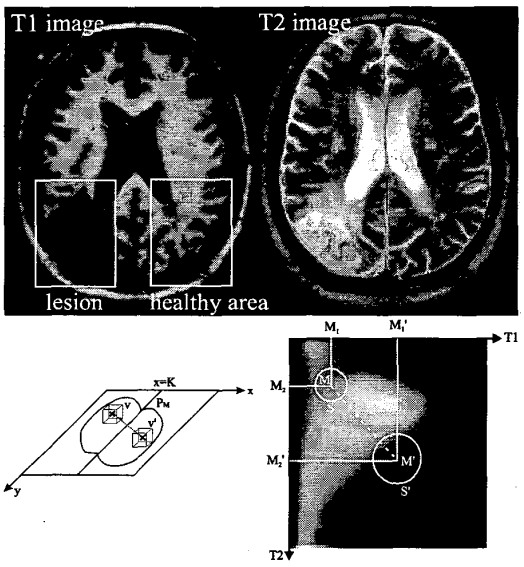

Figure 1: Top: A typical unilateral lesion as revealed by a T_1 (left) and a T_2 weighted (right) MR image. Lesions are detected as significant differences in the signal statistics between small homologeous subregions (below).

As a first approximation, the brain is mirror-symmetric with respect to the mid-sagittal plane. Unilateral lesions should be detectable as symmetry violations of a certain extent (see Fig. 1). Thus, the core idea of the segmentation method proposed here is to compare the signal statistics between both brain hemispheres. In more detail, the processing chain consists of 4 steps:

1. *Preprocessing*: In order to enhance the sensitivity of lesion detection, we employ high-resolution T_1-weighted datasets (Bruker 3.0 T Medspec 100 scanner system, 3D MDEFT protocol, FOV 220x192x220 mm, matrix 256x128x256, voxel size 0.86x1.5x0.86 mm) and T_2-weighted datasets (20 axial slices, FOV 250x250 mm, matrix 512x512, voxel size 0.48x0.48x7.0 mm). First, T_1-weighted images are interpolated to an isotropical voxel size of 1 mm and aligned with the stereotactical coordinate system [10]. Then, an affine transformation determined by a voxel-based registration algorithm is used to align the T_2-weighted image with the high-resolution dataset.

2. *Computing the lesion probability map (LPM)*: A focal lesion is typically confined to a single hemisphere, while the homologeous area on the contralateral side is healthy. The lesion segmentation problem may therefore be stated as finding compact areas with an intensity statistic that differs significantly from the contralateral side.

   Denote by V a small subregion and by V' a corresponding region on the contralateral side. The matrix X (resp. X') contains the $p = 2$ measurements (T_1 and T_2-weighted data) from the n voxels of both subregions (see Fig. 1). A Hotelling T^2 test is used to compare the intensities between V and V':

   $$T = (M - M')^T S_p^{-1} (M - M'), \qquad (1)$$

   where M, M' correspond to the vectors of means in the regions and S_p to the pooled covariance matrix:

   $$S_p = \frac{1}{2(n-1)} (X^T X + X'^T X'). \qquad (2)$$

   The Hotelling T-score is related to an F-score by:

   $$F = \frac{n(2n-p-1)}{2p(2n-2)} T. \qquad (3)$$

   Finally, F-scores are converted into Z-scores and compiled in a map.

   The 3D volume is scanned, and for each pair of subregions a Z-score is calculated. A sign is addressed to the Z-values that depends on the sign of the components of the matrix $M - M'$. We obtain therefore a 3D lesion probability map where areas with high signal asymmetries are depicted by high Z-scores.

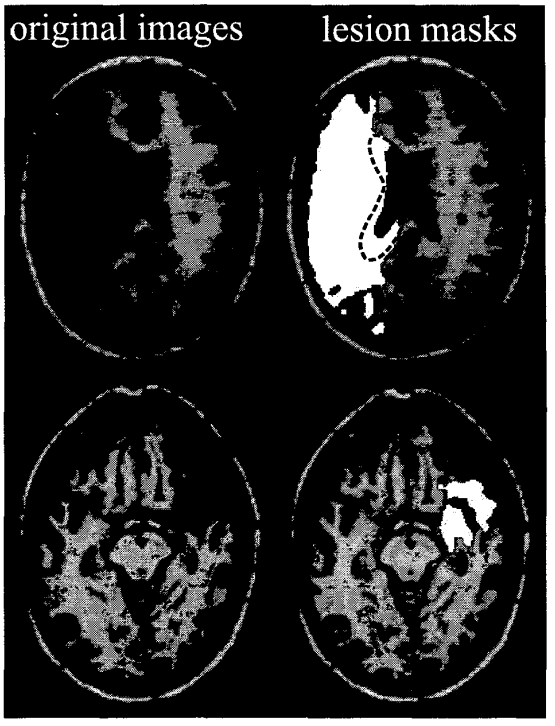

Figure 2: The advantage of this lesion detection method is that it depicts the *whole* tissue loss, e.g. by including parts of the consequitively enlarged ventricle (top), but spares anatomical sulci (below).

3. *Post-processing*: Since we perform a voxel-wise test, we must correct for the multiple comparison problem before addressing a significance to a connected region representing a possible lesion. We apply an equation that was proposed in the context of functional MRI data analysis [4]. LPMs are thresholded by a certain Z-score, and the size of all connected components is computed. Based on the component size, the size of the search region (i.e., the brain) and the smoothness of the LPM, a probability is addressed to a connected component. If this probability is below a pre-set threshold (e.g., $p < 0.05$) then we accept this connected component as a probable lesion. Non-significant regions typically contain less than 10 voxels. The behavior of the algorithm is demonstrated here on two cases (see Fig. 2). The lesion borders depend obviously on the threshold value Z. If it is too low, the lesion might be overestimated, otherwise it would be underestimated.

The method is straightforward to implement, fast and robust. Using a statistical framework for lesion definition is

expected to yield more consistent and better reproduceable results than manual or semi-automated procedures.

3. SEGMENTATION OF MULTIFOCAL SMALL LESIONS

Enlarged Virchow-Robin spaces (VRS) correspond to small gaps between the white matter and its supplying deep penetrating arteries. They appear as small tubular structures filled with cerebro-spinal fluid (CSF) that (ideally) are radial to the brain surface. Typically, they are close to the spatial resolution limit of current MRI methods (1-3 mm in diameter and 3-15 mm long), and a single brain may contains hundreds of such lesions. So far, these lesions are evaluated visually in the acquired data sets and rated by semiquantitative scales [11].

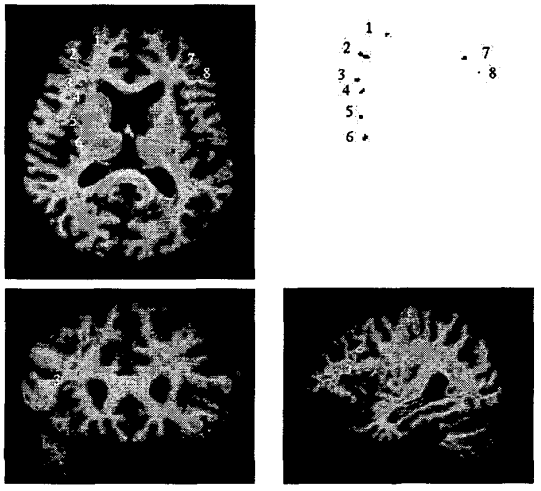

Figure 3: An example of VRS detection: (a) Original axial slice, (b) detected VRS, (c) Coronal slice corresponding to VRS 3, (d) Sagittal slice corresponding to VRS 3.

Structure and distribution of VRS have motivated the following approach. Firstly, a VRS typically represents several voxels forming a tubular shape (see Fig. 3). Thus, an approach based on a geometrical object appears suited for this problem. Secondly, VRS are not uniformly localized and some regionally higher occurence can be observed. Interactions between objects were included in the model to favor clustering of VRS while suppressing an overlap of different VRS.

The template theory introduced by Grenander allows modeling random shapes [5]. Here, the object's shape model is simple and will be represented by a small segment. The complexity of the model lies in the different object interactions we will introduce. Therefore, we have preferred the marked point process framework here [1]. A point process defined with a Poisson density measure models the number of objects and their localization in the scene. This process may include interactions between points such as explicit relations or clustering properties. Shape parameters are associated with the points to define the object geometry (e.g., length and orientation of an object). A certain shape variability (length and diameter of the tubular structures in our case) and data noise have to be taken into account that introduce local minima of the cost function related to the model. To overcome this problem, we consider a stochastic framework. Model optimization can be achieved by an Reversible Jump Markov Chain Monte Carlo algorithm (RJMCMC) [3] embedded in a simulated annealing scheme.

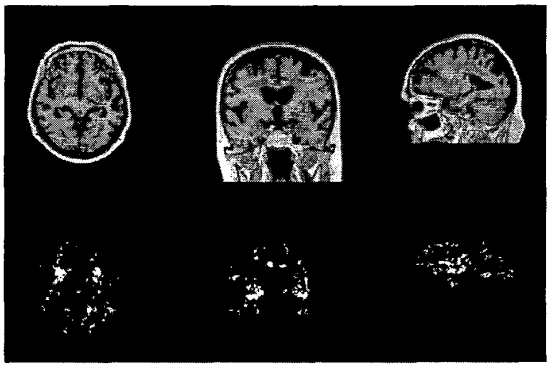

Figure 4: Cumulative spatial distribution of VRS collected from 37 datasets, together with the reference brain. A higher prevalence of VRS is found in the area supplied by the medial and lateral striate arteries (e.g., putamen and pallidum) and in the area supplied by the long penetrating arteries, especially in the frontal white matter compartment.

First, results are presented for a particular dataset that has been selected among cases with a high prevalence of VRS. Figure 3 shows sample orthogonal slices and their detected lesions. To achieve an idea about the spatial distribution of VRS, 37 brain datasets of elderly people were analyzed by this procedure and registered to the same brain using a non-linear procedure based on fluid dynamics. The obtained displacement fields were used to transform the detected VRS into a common space. Figure 4 shows the cumulative spatial distribution of VRS collected from all datasets, together with the reference brain. A higher prevalence of VRS is found in the area supplied by the medial and lateral striate arteries (e.g., putamen and pallidum) and in the area supplied by the long penetrating arteries, especially in the frontal white matter compartment.

4. SEGMENTATION OF DIFFUSE BRAIN LESIONS

Changes in the cerebral hemispheric white matter are often detected in MRI brain datasets of elderly persons [12]. The pathogenesis, clinical significance and morphological substrate of these changes are incompletely understood [2]. In order to deduce the clinical significance of these findings, it is necessary to derive quantitative descriptors for them. The usual clinical practice is to evaluate images visually on the basis of a semi-quantitative rating scale [11]. Using texture features to segment diffuse white matter hypointensities (DWMH) appears a worthwhile and attractive approach.

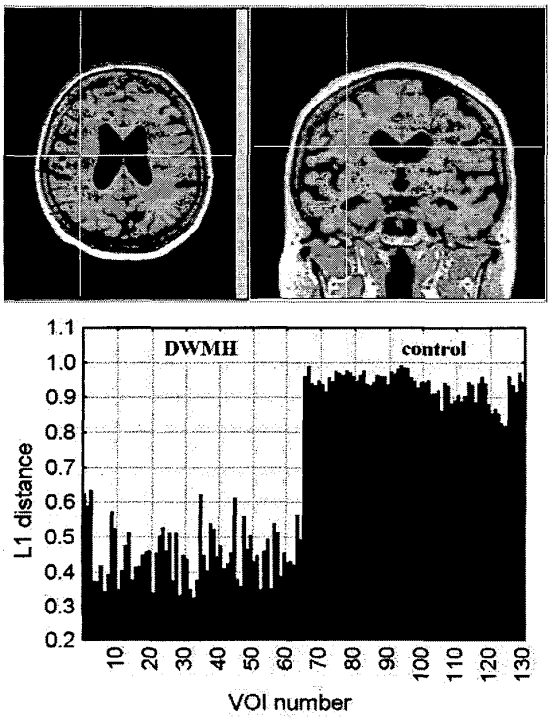

Figure 5: Calculation of a representative co-occurrence matrix for segmentation of DWMH. (a) Typical example of DWMH sample region defined as 7x7x7 mm VOI with the center pointed out by crossing lines. (b) Distances to the mean lesion co-occurrence matrix for 65 lesion and 65 control VOIs.

We suggested using 6-dimensional co-occurrence matrices [8] for describing regional texture features that are comprised of intensities $I(i), I(j)$ of voxel pairs, their gradients $G(i), G(j)$, the angle between gradients $a(i,j)$, and their distance $d(i,j)$. For this example, dimensions were binned as follows: 4 intensity bins (64 units each), 6 angle bins (30 degrees each), 4 distance bins ($d = 1 - 4mm$). Co-occurrence matrices are collected within a certain volume-of-interest (VOI), and represented as a point in the 6-dimensional feature space. Texture-based segmentation can be performed in four steps:

1. *Calculating a representative lesion descriptor*: A training set that includes VOIs representing sample lesion regions and corresponding control regions is constructed. Selecting a proper VOI size is a compromise: it must be big enough to capture the typical pattern of the lesion, but small enough to provide a reasonably precise segmentation of the lesion borders. Since image VOIs are supposed to be of the same size, there is no need to normalize co-occurrence descriptors. The representative descriptor can be calculated as an average matrix over the lesion image VOIs given in the training set.

2. *Selecting a similarity metric*: The purpose of this step is to select and tune a suitable function that maps distances between the current and representative VOI descriptors into a lesion probability map. A suitable choice is a simple L1 norm that addresses a nonzero probability to distances found for lesion samples and zeros for distances close to control VOIs:

$$L1(V^l, V^c) = \frac{\sum_{i=1}^{N} |v_i^l - v_i^c|}{\sum_{i=1}^{N} v_i^l + \sum_{i=1}^{N} v_i^c}, \qquad (4)$$

   where v_i correspond to the elements of the co-occurrence matrix of the lesion and the control regions. Note that control VOI samples are included for this tuning process only.

3. *Segmentation*: An image is scanned with a given VOI size, calculating the distance from the current VOI to the representative one in feature space and addressing a corresponding probability label to the central voxel of the current VOI. Thus, a voxel of the probability map corresponds to the similarity of a neighborhood with the lesion VOI.

4. *Post-processing of the probability map*: It is unlikely that all image VOIs within the box-shaped scanning area are consistent with respect to the lesion similarity criteria. Therefore, some post-processing is necessary to remove false-positive map labels outside of the typical lesion space (here, the WM compartment).

Experimentation revealed a VOI size of 7x7x7 mm to be adequate. The training set was formed from 3 patient and 4 control datasets and included 65 DWMH and 65 control VOIs. Figure 5 shows example slices of a patient dataset and the L1 mapping in feature space. To compute DWMH probability maps, a linear mapping of the distance to the label range 0-255 was used, where the maximal value 255 was associated with 0.42 (mean distance over 65 DWMH

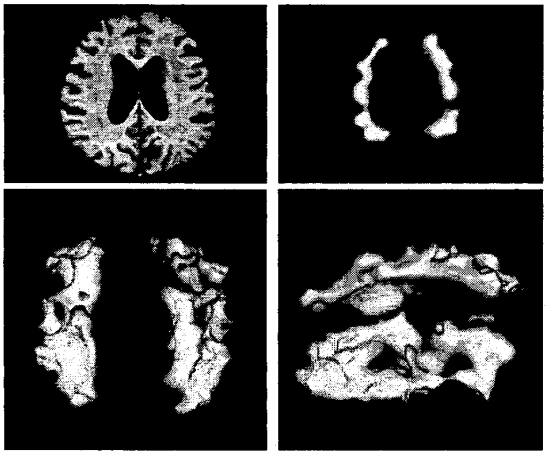

Figure 6: Result of the DWMH segmentation. (a) Original image slice. (b) Probability map of the lesion for the slice depicted in (a). (c)-(d) Two directly rendered views of the 3-D lesion map.

VOIs) and the minimal label 0 with 0.69 (mean distance between both VOI classes).

Figure 6 shows example segmentation results as 2-D sections of the probability map for a reference image slice (upper row) and two 3D rendered views of the map (bottom). Lesion maps produced by this technique have a voxel-by-voxel correspondence with the original brain dataset and can be used for a quantitative estimation of lesion severity.

5. SUMMARY

Three methods were described for the detection of large unilateral brain lesions, small multifocal lesions and diffuse lesions of the brain's white matter. All methods were tested on a large number of clinical cases, and have proven their reliability. Their use may be considered as supplementary information of a clinical report, in statistics for clinical trials or therapeutic monitoring.

6. REFERENCES

[1] A.J. Baddeley and M.N.M. van Lieshout, Stochastic geometry models in high-level vision. *J. Appl. Stat.* 20, 231-256 (1993).

[2] M.M.B. Breteler, N.M. van Amerongen, J.C. van Swieten, J.J. Claus, D.E. Grobbee, J. van Gijn, A. Hofman and F. van Harskamp, Cognitive correlates of ventricular enlargement and cerebral white matter lesions on magnetic resonance imaging: The Rotterdam study, *Stroke* 25, 1109-1115 (1994).

[3] X. Descombes, R. Stoica, L. Garcin and J. Zerubia, A RJMCMC Algorithm for Object Processes in Image Processing. *Monte Carlo Methods and Applications* 7, 149-156 (2001).

[4] K.J. Friston, K.J. Worsley, R.S.J. Frackowiak, J.C. Mazziotta and A.C. Evans, Assessing the significance of focal activations using their spatial extent, *Human Brain Mapping* 1, 210-220 (1994).

[5] U. Grenander, *General Pattern Theory*, Oxford University Press, Oxford (1993).

[6] S.A. Hojjatoleslami and F. Kruggel, Segmentation of large brain lesions. *IEEE Trans. Med. Imag.* 20, 666-669 (2001).

[7] M. Kamber, R. Shinghai, D.L. Collins, G.S. Francis and A.C. Evans, Model-based 3-D segmentation of multiple sclerosis lesion in magnetic resonance brain images. *IEEE Trans. Med. Imag.* 14, 442-453 (1995).

[8] V.A. Kovalev, F. Kruggel, H.J. Gertz and D.Y. von Cramon, Three-Dimensional Texture Analysis of MRI Brain Datasets, *IEEE Trans. Med. Imag.* 20, 424-433 (2001).

[9] S. Loncaric, A.P. Dhawan, D. Cosic, D. Kovacevic, J. Broderick and T. Brott, Quantitative intracerebral brain hemorrhage analysis, *Proc. SPIE* 3661, 886-894 (1999).

[10] F. Kruggel and D.Y. von Cramon, Alignment of magnetic-resonance brain datasets with the stereotactical coordinate system, *Medical Image Analysis* 3, 175-185 (1999).

[11] P. Scheltens, T. Erkinjunti, D. Leys, L.O. Wahlund, D. Inzitari, T. del Ser, F. Pasquier, F. Barkhof, R. Maentylae, J. Bowler, A. Wallin, J.Ghika, F. Fazekas and L. Pantoni, White matter changes on CT and MRI: an overview of visual rating scales, *Eur. Neurol.* 39, 80-89 (1998).

[12] L. Pantoni and J. H. Garcia, The significance of cerebral white matter abnormalities 100 years after Binswanger's report: A review, *Stroke* 42, 1293-1301 (1995).

[13] A.P. Zijdenbos, B.M. Dawant, R.A. Margolin and A.C. Palmer, Morphometric analysis of white matter lesions in MR images: Method and validation, *IEEE Trans. Med. Imag.* 13, 716-724 (1994).